King Saud University

**Arabian Journal of Chemistry**

www.ksu.edu.sa
www.sciencedirect.com

# ORIGINAL ARTICLE

# HPMC crosslinked chitosan/hydroxyapatite scaffolds containing Lemongrass oil for potential bone tissue engineering applications

**Hafiz U. Ali [a], Dure N. Iqbal [a], Munawar Iqbal [b],\*, Safa Ezzine [c,d], Aysha Arshad [e], Rabia Zeeshan [e], Aqif A. Chaudhry [e], Samar Z. Alshawwa [f],\*, Arif Nazir [a], Ather F. Khan [e],\***

[a] *Department of Chemistry, The University of Lahore, Lahore, Pakistan*
[b] *Department of Chemistry, Division of Science and Technology, University of Education, Lahore, Pakistan*
[c] *Department of Chemistry College of Sciences, King Khalid University, P.O. Box 9004, Abha, Saudi Arabia*
[d] *Laboratoire des matériaux et de l'environnement pour le développement durable LR18ES10, 9 Avenue Dr.Zoheir Safi, 1006 Tunis, Tunisia*
[e] *Interdisciplinary Research Centre in Biomedical Materials, COMSATS University Islamabad, Lahore Campus, Pakistan*
[f] *Department of Pharmaceutical Sciences, College of Pharmacy, Princess Nourah bint Abdulrahman University, P.O. Box 84428, Riyadh 11671, Saudi Arabia*

**Abstract**  The chitosan (CS), hydroxypropyl methyl cellulose (HPMC), hydroxyapatite (HAp and Lemon grass oil (LGO) based scaffolds was prepared by freeze gelation method. The composite formation was confirmed by FTIR (Fourier-transform infrared spectroscopy) analysis and surface morphology was evaluated by SEM (Scanning Electron Microscopy) analysis. The mechanical strength, biodegradation, swelling, porosity and antibacterial activity were evaluated on the basis of LGO contents. The scaffold structure was porous and the mechanical strength was enhanced as a function of LGO contents. The scaffold properties analysis revealed the biodegradation nature and swelling behavior of CS-HPMC-HAp-LGO was also affected significantly as a function of LGO contents. The cytotoxicity of CS-HPMC-HAp-LGO was studied against MC3T3-E1 cells and based on cell viability, no toxic sign was observed. The antimicrobial activity was evaluated against *S. aureus* and CS-HPMC-HAp-LGO scaffolds showed promising activity, which was varied

\* Corresponding authors.
  E-mail addresses: bosalvee@yahoo.com (M. Iqbal), szalshawwa@pnu.edu.sa (S.Z. Alshawwa), atherfarooq@cuilahore.edu.pk (A.F. Khan).
Peer review under responsibility of King Saud University.

**Production and hosting by Elsevier**

as a function of LGO contents. The findings revealed that the CS-HPMC-HAp-LGO are biocompatible and have potential for bone tissue engineering.

## 1. Introduction

The bone disorders like osteoporosis, Paget's disease, and periodontitis are caused by an imbalance in bone healing, which is typically due to massive bone resorption compared to bone formation (Sanjay et al., 2017). Bone grafting is useful for reconstruction of bone defects. Conventionally, allografts and autografts have been used, however, despite the risk of disease spread and limitations, biomaterials-based bone substitutes are highly effective (Chen and Jin, 2010). According to physiochemical and biomechanical requirements, bioactive and biocompatible composite scaffold materials have been produced as a substitute to overcome many medical exigencies, i.e., donor unavailability, inadequate immunological response and infection proliferation. The scaffold made of synthetic polymer face serious issue of residual non-biocompatibility, this is because of cytotoxic material used during their fabrication that may cause toxicity to the cell and tissues. The NO overproduction, ROS-induced oxidative stress, mitochondrial malfunction (Eftekhari et al., 2018; Asghar et al., 2021), and DNA damage have all been identified as major cell toxicity mechanism. Recent research has revealed that mitochondrion malfunction and oxidative stress frequently coexist in toxicant that induced cell toxicity, and they may be used to avoid cell toxicity (Wu et al., 2018). Scaffolds having antioxidant and antibacterial properties promote wound healing and are being considered as a possible tissue engineering material for chronic wounds (Asghar et al., 2021; Abbasi et al., 2020). Antioxidants seem to eliminate the influence of oxidative stress on the bones (Abbasi et al., 2020). The most recently and interesting discovered, nano-encapsulated antioxidant molecules. Nanoscale technologies, as scientific drivers of innovation, have provided a positive perspective by identifying nano-antioxidant substances using various methodologies (Eftekhari et al., 2018). The bone tissue engineering (BTE) incorporates aspects of biology, bioengineering, and materials science to create tissue construct known as scaffolds, which act as bone substitutes and has a significant role in bone repairing and maintenance in deformed or bone diseases (Balagangadharan et al., 2017; Saravanan et al., 2016). Substituted scaffold should also be porous, nontoxic, biocompatible, facilitate cell differentiation, cell attachment and degrade according to new tissues formation, promote metabolites movement as well as fill voids at the implantation sites. They should be osteoinductive as well as promote osteo-conduction and also mimic natural micro-environment at the implantation sites (Shuai et al., 2018; Feng et al., 2019).

The HAp $(Ca_{10}((PO_4)_6(OH)_2)$ comprises 65 percent (approximately) of inorganic component of natural bone. It shows a strong affinity for tissues that stimulate bone growth (Heise et al., 1990; Shuai et al., 2021; Shuai et al., 2021). Several researches revealed that solid HAp show its biocompatibility with natural bone tissues (Panda et al., 2021; Ressler et al., 2021). Hence, researchers are exploring the role of HAp in guided bone regeneration. Clinical practice and biological research have demonstrated that 3D scaffold with interconnected pores are a favorable tool for bone regeneration. These characteristics result in improved proliferation, differentiation, cellular attachment and a network that ensures nutrition movement. It has been extensively studied in biomedical applications due to its suitable mechanical stability and osteo-conductive. Therefore, owing to its low resorption rate, HAp applications is confined as a bone filler. Ceramic materials have limitations that can be mitigated by blending ceramics with polymers. These composites have been found to be useful in a number of ways, including more controls over the structure of the scaffold, enhancing bone tissue bonding, adaptability and clotting formation enhancement (Feng et al., 2019; Feng et al., 2018).

Recently, lot of studies have been focused on a biomaterial-based constructs made of synthetic and natural polymers for prospective clinical use. Among natural polymer, chitosan (CS) is a polysaccharide produced from the deacetylation of chitin, which is primarily a constituent of crustacean exoskeletons (Hong et al., 2017). Chitin, when deacetylated, becomes positively charged under week acidic conditions due to the existence of primary amine groups, a distinctive feature attributed to CS (Giotra et al., 2015). The role of CS in drug delivery and tissue engineering has been widely reported because of its biocompatibility. Several studies have highlighted the CS-based applications of different materials. HPMC (hydroxypropyl)methyl cellulose) is water soluble, nontoxic, natural polymer with a number of desirable characteristics (Siepmann and Peppas, 2012), i.e., H-bonding for interaction of CS with HPMC (Pawlak and Mucha, 2003). HPMC, which is a biodegradable polymer that is widely utilized in the fabrication of formulations with controlled release systems that has been approved by the US Food and Drug Administration (Mahmoudian and Ganji, 2017). Thermosensitive CS-HPMC hydrogels have also been developed for potential application in the biomedical field. Furthermore, the potential function of cellulose for bone tissue engineering in association with HAp has been highlighted in several studies that have been utilized different polysaccharides in combination with cellulose (Heise et al., 1990; Shuai et al., 2021; Shuai et al., 2021; Ahmadian et al., 2019).

Essential oils (EOs) derived from plants are natural microbial agents; their integration into composite polymers may not only improve the antibacterial characteristics of the material, but also lower its water solubility, vapor permeability, and decrease lipid oxidation (Hafsa and M. ali Smach, M.R.B. Khedher, B. Charfeddine, K. Limem, H. Majdoub, S. Rouatbi, , 2016; Stegăruş and Lengyel, 2017). The EOs are prospective candidates for the treatment of osteoarthritis due to their anti-inflammatory, antiproliferative, antioxidant, and antiangiogenic properties (Jian-Ping et al., 2018). Furthermore, EOs might be used as bioactive components in scaffolds developed for bone tissue regeneration. Similarly, EOs might be used to coat metallic implants to avoid microbial contamination and infection. The electrospun polyurethane was treated with lavender essential oils and cobalt nitrate, and the studies exhibited prolonged blood coagulation, nontoxic behaviour on fibroblast cells, and bone mineralization characteristics (Zhang et al., 2019). The natural and synthetic materials such as hydroxyapatite (HAp) and collagen (Coll) were also combined with EOs such as eucalyptus essential oil to prepare scaffolds for bone regeneration application (Florea et al., 2018). Before present investigation, the use of HPMC as mediator in the fabrication of CS/nano-HAp scaffolds has been reported (Khan et al., 2015). To advance it further, the Lemongrass oil (LGO) is incorporation into CS/HAp/HPMC to fabricate different composite scaffold of CS-HAp-HPMC-LGO by freeze-gelation. The effect of LGO contents was studied on the basis of porosity, mechanical strength, swelling behavior and degradation of CS-HAp-HPMC-LGO. The antimicrobial activity was also studied of CS-HAp-HPMC-LGO.

## 2. Material and methods

### 2.1. Chemical/reagents

The HPMC (BDH, UK), absolute ethanol, CS (Merck, Germany), hydroxyapatite (HAp, sintering grade) (Plasma Biotal Ltd., UK), phosphate buffer saline tablets (PBS, Sigma-

Aldrich, Germany), lysozyme (Sigma-Aldrich, Germany), base media Alpha Minimum Essential Medium (α-MEM) (Gibco Catalog No. A1049001), Span 80 (surfactant), nutrient agar, fetal bovine serum (FBS), antibiotic amikacin, penicillin/streptomycin, trypsin and cell culture grade PBS were purchase from Gibco (Thermo-Fisher scientific) and Alamar Blue assay Reagent (Sigma-Aldrich, Germany) was used. All the chemicals were analytical grade and used without further purification.

## 2.2. Synthesis of CS-HPMC-HAp-LGO

A series of different combinations of CS-HPMC-HAp-LGO composite scaffolds were synthesized, each scaffold composition is depicted in Table 1 and schematic is given in Fig. 1. Freeze gelation method (Ressler et al., 2020) was used for scaffold preparation. All four components, CS, HAp, HPMC and LGO were mixed, for this, CS was first dissolved in 1.6 wt% acetic acid in water (25 mL) by stirring for half an hour. After mixing CS, HPMC had been added and mixed at room temperature and stirred it for 30 min. Then, HAp was added along with stirring for 8 h, which furnished a dense slurry. Then, the different LGO contents (wt.%) was added to the slurry along with surfactant with constant stirring. The blend was sonicated to promote elimination of bubbles before adding slurry to the molds. The molds were placed in freezer first at $-20$ $^0$C for three h and then, transfer to $-40$ $^0$C for 24 h. After 24 h, the scaffolds were freeze with 3 M NaOH in ethanol solution for gelation formation for 48 h, which are washed with ethanol and deionized water for the elimination of acidic as well as basic residues and then under sterile environments, the samples were dried and subjected to further analysis.

## 2.3. FTIR and surface morphology analysis

Scanning electron microscopy is the best method for studying surface morphology of materials since it uses a high intensity electron beam to examine the material. The microstructure and surface morphology of CS-HPMC-HAp-LGO scaffolds were studied by using an FEI-NOVA-450 nano SEM (FE-SEM), USA. The SEM-EDS micrograph explain surface modification and porosity of the sample. The intermolecular interaction among components was studied by FT-IR. A FT-IR NICOLET 6700, Thermo Scientific spectrometer was used to record the spectra of bio-composite scaffolds Table 2. The spectra were obtained between 650 and 4000 cm$^{-1}$.

## 2.4. Mechanical analysis

Mechanical testing is difficult without holding the sample correctly in case of porous composite ceramic scaffolds.

Conventional methods such as biaxial, tensile including impact testing are therefore inappropriate (Currey and Butler, 1975). For cancellous bone as well as porous analysis of HAp, only compression tests have been reported and widely accepted (Hing et al., 1999; Hodgskinson and Currey, 1990). The compression mechanical analysis as per ASTM D5024-95a guidance was carried out by an electrodynamic fatigue testing Machine (Walter + bai AG, Switzerland) with a 1.5 kn loaded cell. The speed of the crosshead was adjusted to 0.5 mm/min, and load was applied on sample height up to 35% reduction. Samples for compressive strength were examined.

## 2.5. Biodegradation analysis

The biodegradation study of the composite scaffold was conducted in the presence of 100 μg/mL lysozyme solution (20,000 U/mL) in PBS medium at 37 °C. The test was carried out by immersing samples (CS-HPMC-HAp-LGO) in the lysozyme-containing PBS and incubating them for various time periods (1–14 days. Samples were separated from media after each period and washed with deionized water to eradicate ions which are adsorbed on the surfaces and then dried using filter paper and vacuum drying oven. Initial scaffold weight was observed as $W_i$ and $W_d$ was observed as the dry scaffold weight. The percentage of scaffold degradation was determined by employing Eq. (1).

$$\text{Degradation}(\%) = \frac{W_i - W_d}{W_i} \times 100 \tag{1}$$

## 2.6. Swelling studies

Swelling studies were examined at pH 7.4 at 37° C for 24 and 48 h in the PBS. The scaffold dry weight was recorded ($W_d$). Scaffolds were removed after each specific time period. Filter paper was used to eliminate the adsorbed water, then wet weight ($W_w$) was measured. The swelling ratio was estimated by employing Eq. (2).

$$\text{Swelling ratio} = \frac{W_w - W_d}{W_d} \tag{2}$$

## 2.7. Porosity analysis

Porosity is known as the void fraction in the sample and is a morphological feature that is independent from the biomaterial. Liquid displacement method was used to measures the porosity with absolute ethanol (Khan et al., 2015; Ressler et al., 2020). Ethanol (0.789 g/cm$^3$) was used as displacement media and did not alter the size of the pores. Briefly, a piece

**Table 1** Composition of CS-HPMC-HAp-LGO porous composite scaffolds.

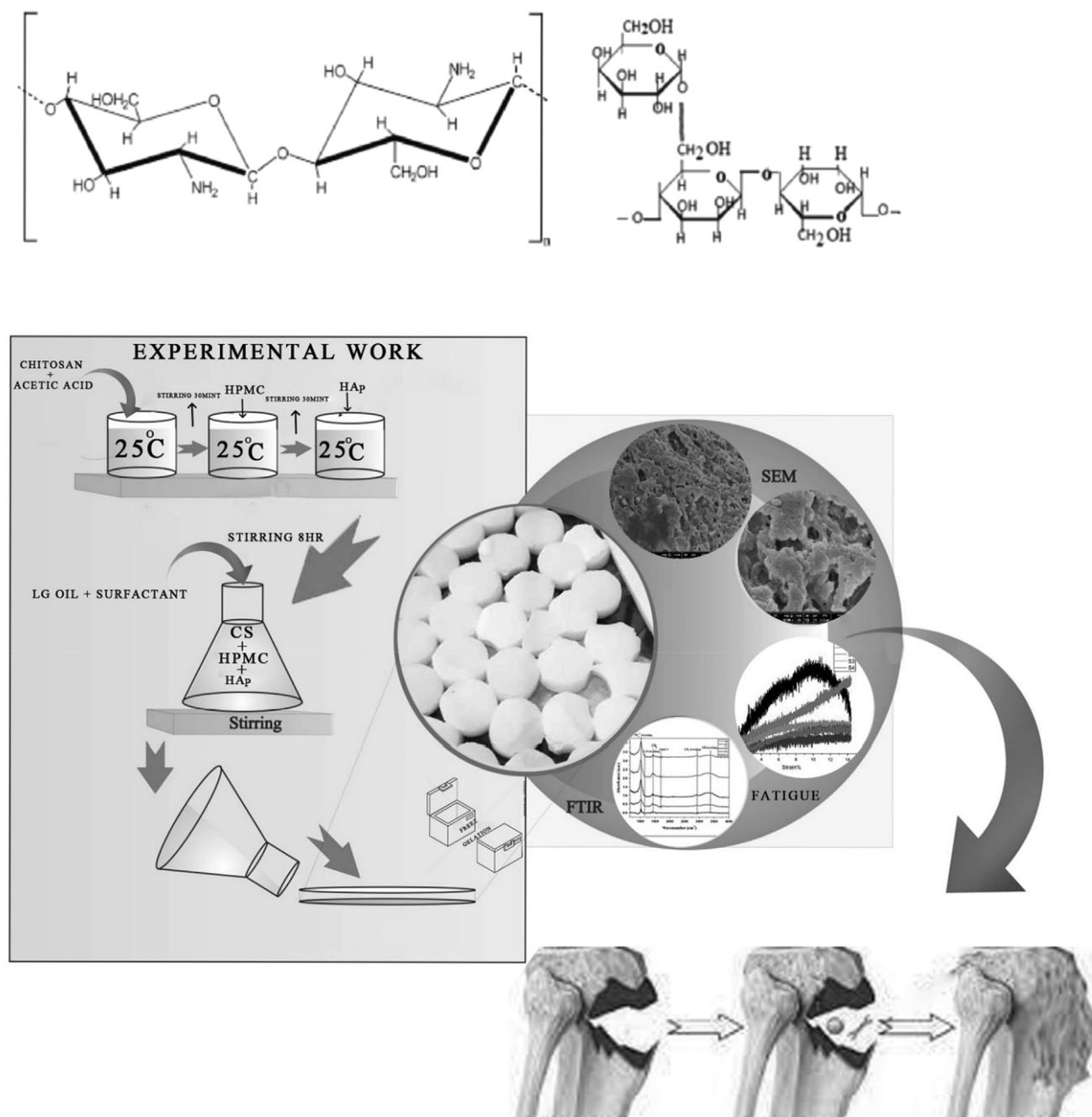| Sr. No. | CS/HAp/HPMC/ LG essential oil with Wt.% ratio | | | |
| --- | --- | --- | --- | --- |
| | HAp | CS | HPMC | LG oil |
| C | 1.25 (42%) | 1 (33%) | 0.75 (25%) | – |
| S-1 | 1.25 (42%) | 1 (33%) | 0.75 (25%) | 0.5 (0.5%) |
| S-2 | 1.25 (42%) | 1 (33%) | 0.75 (25%) | 1 (1%) |
| S-3 | 1.25 (42%) | 1 (33%) | 0.75 (25%) | 1.5 (1.5%) |
| S-4 | 1.25 (42%) | 1 (33%) | 0.75 (25%) | 2 (2%) |

**Fig. 1**    Schematic presentation of CS-HPMC-HAp-LGO composite.

of scaffold ranging ($1 \times 1 \times 1$ mm$^3$) was dipped into 20 mL ethanol of specific volume ($V_1$). After incorporation of the scaffold in ethanol, the raised ethanol volume was recorded as $V_2$. After 30 min, the scaffold was removed, the volume of residual ethanol was recorded as $V_3$. Ultimately, the scaffold percentage porosity ($\varepsilon$) was measured by employing Eq. (3) and the density of composite scaffold was determined by applying Eq. (4).

$$\text{Porosity}(\%) = \frac{V_1 - V_3}{V_2 - V_3} \times 100 \qquad (3)$$

$$\text{Density} = \frac{\text{Weight}}{V_2 - V_3} \qquad (4)$$

### 2.8. Antibacterial activity

The antibacterial activities were tested by turbidimetric method with slightly modifications. The sample were cut in the form of discs and sterilized with UV radiation. *S. Aureus* bacteria was cultured and adjusted to get optical density (OD 600 nm) according to corresponding $\sim$10$^6$c.f.u. *S. Aureus* were placed for 2, 6 and 24 h in 5 mL of 10$^6$c.f.u/ml on an orbital blender at 37 $^0$C, and measured absorbance through UV visible spectrophotometer after 2-, 6- and 24-hours incubation, and with the given formula the percentage viable cell was calculated. The sample was not added to bacterial suspension for negative control, while bacterial suspensions was incubated

with commercial antibiotic disc in order to ensure the positive control. The evaluation of percentage viable cell in CFU/mL determined the bacterial viability, in which bacterial suspension cell viability without the sample was chosen as the cell viability of 100 %. The evaluation of all sample was done in triplicates.

$$Viability\ of\ bacterial\ cell\ (\%) = \frac{OD(sample)}{OD(Blank)} \times 100 \qquad (5)$$

### 2.9. Cytotoxicity studies

The cell viability of MC3T3-E1 cells line was measured on scaffold disks using Alamar Blue assay. It is a non-fluorescent dye that acts based on mitochondrial reduction of living cells. The amount of living cells is proportional to the quantity of florescence produced (Shalumon et al., 2011). Composite scaffold was initially incubated for 10 min in culture medium, before cell seeding to wet the scaffold surface. The MC3T3-E1 cells were allowed to cultivated in five various scaffolds for 1, 3 and 7 days. After each expiry culture duration, a 10% Alamar Blue medium was introduced to each 24 well plate that containing scaffolds and was placed it for 4 h incubation. After 4 h, media comprising Alamar blue was removed from each well, and solution absorbance was read at 620 nm using microplate reader of Labtech LT 4500. It

was performed for each scaffold in triplicate and as a control TCP was added.

$$Viability\ of\ cell\ (\%) = \frac{OD_{620}(Sample)}{OD_{620}(Blank)} \times 100 \qquad (6)$$

### 2.10. Statistical analysis

All experiments were performed in triplicate and data is given in the form of the mean $\pm$ standard deviation (SD).

### 3. Results and discussion

#### 3.1. Surface and composition

SEM-EDS images of cross-sectional microstructures of CS/HA/HPMC/LGO composite scaffolds, including pore morphology and distribution as shown in Fig. 2. As can be observed, the CS-HPMC-HAp-LGO composite scaffold had a compact and smooth microstructure when compared to the control, as predicted for a homogeneous composite. This demonstrates the component's high compatibility. Researches have shown that due to incorporation of essential oil (EOs) to the biopolymer composites, increases the roughness, compactness and more cavity are appeared without cracks due to
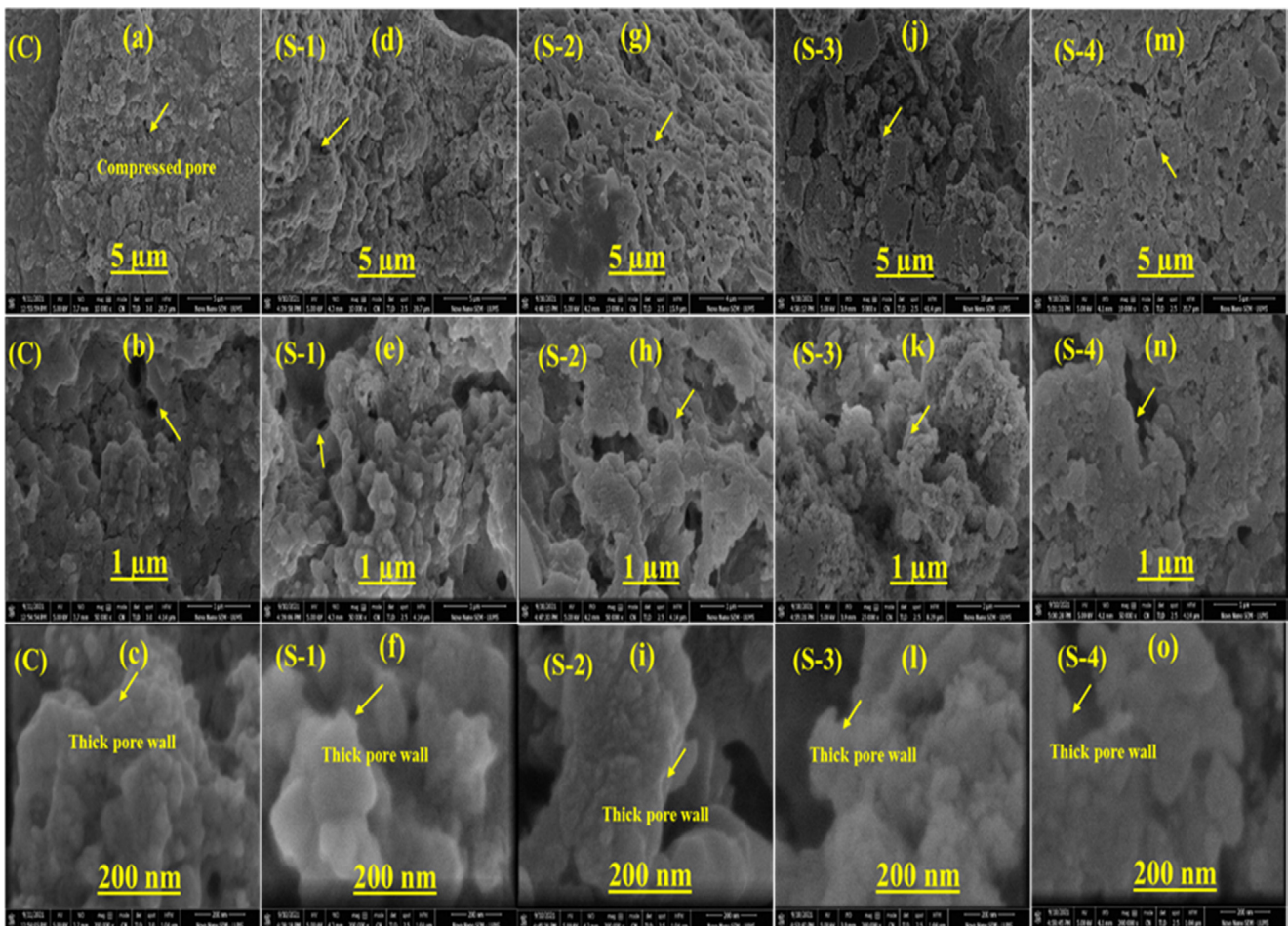


**Fig. 2** SEM images of an CS-HPMC-HAp-LGO composite scaffolds.

hydrophobicity of EOs (Amalraj et al., 2020). Similarly, when an increase in concentration of hypericum oil and thyme oil in the chitosan film resulted in a more porous structure with uniformly distributed pores (Altiok et al., 2010; Güneş and Tıhmınlıoğlu, 2017). In comparison to the CS-HPMC-HAp control, the surface microstructure of the CS-HPMS-HAp-LGO composite scaffold containing 0.5% LGO had no fractures. This shows that the LGO was successfully dispersed in the CS-HPMC-HAp matrix at extremely low concentrations by developing very tiny droplets with great surface areas, with negligible impact on Scaffold homogeneity. However, the presence of 1% LGO affected the homogeneity of the microstructure of composite scaffolds, causes roughness and uneven surfaces. The pore wall and pore size morphology can be changed by better crosslinking. The surface microstructure of S-3 and S-4 become more heterogeneous due to 1.5% and 2% of LGO respectively. This is because of coalescence and aggregation of oil droplet embedded in CS-HPMC-HAp-LGO composite scaffold. Similarly, Song et al. (Song et al., 2018) found that increasing the percentage of lemon EO from 0.5 to 1.5 % enhanced the surface heterogeneity and roughness of corn and wheat starch films. Moreover, the compact microstructure may increase the pore wall thickness and decrease the pore size. Similar research found that the incorporation of RGEO in a concentration dependent way to the CS matrix increased the thickness considerably owing to molecular interaction between CS and RGEO (Grande Tovar et al., (2020) 1688.) which may decrease the pore size. The average diameter of the pores was 119.97 μm for C, 121.44 μm for S-1, 103.88 μm for S-2, 99.48 μm for S-3 and 97.49 μm for S-4. In C used as a control. There were significant variances between the S-1, S-2, S-3, and S-4. The pore wall got thicker, more homogeneous, and compact as the LGO concentration increased, as well as the surface morphology also become rough. The most suitable range of pore size in porous polymer

in combination with HAp for the body fluid and cell to migrate into scaffold and regenerate bone tissues is 85–325 μm (Murphy and O'Brien, 2010).

### 3.2. FTIR analysis

The FTIR spectra of CS-HPMC-HAp-LGO composite scaffold as well as its constituent CS, HPMC, HAp and LGO is shown in Fig. 3. The characteristics frequency value of different functional group in composite scaffold CS-HPMC-Hap-LGO and their pristine CS, HPMC, Hap and LGO are shown in table 2. The FTIR spectrum of pristine HAp demonstrates sharp absorbance between in the range of 1000 cm$^{-1}$ to 1100 cm$^{-1}$ corresponding to $PO_4^{3-}$ ion (Khan et al., 2015; Rehman and Bonfield, 1997; Swain et al., 2011; Mobasherpour et al., 2007). The absorption bands at 1018 cm$^{-1}$, 1019 cm$^{-1}$,1021 cm$^{-1}$ and 1022 cm$^{-1}$ in the spectra of CS-HPMC-HAp-LGO composite scaffolds confirms the occurrence of $v_3$ antisymmetric stretching vibration mode of $PO_4^{3-}$ group of HAp in the sample. $CO_3^{2-}$ is identified in the FTIR spectrum of HAp as an A-type substitute of the HO$^-$ or a B-type substitute of the $PO_4^{3-}$ in the HAp lattice (Antonakos et al., 2007). The existence of $CO_3^{2-}$ bands at 1540 cm$^{-1}$ shows A-type $CO_3^{2-}$, whereas bands at 1410 cm$^{-1}$ indicate B-type $CO_3^{2-}$ (Antonakos et al., 2007; Delgado-López et al., 2012). Furthermore, both types of $CO_3^{2-}$ substitution are responsible for a weaker broad shoulder in the 870 cm$^{-1}$ – 880 cm$^{-1}$ range (Meejoo et al., 2006). The absorption band for A type $CO_3^{2-}$ is moved to a higher frequency in the CS-HPMC-HAp-LGO composite, probably due to interaction with CS, HPMC, and LGO. Contrary, $CO_3^{2-}$ substitutes of B-type is accompanied with a weak absorption band at 875 cm$^{-1}$. These results indicate that $CO_3^{2-}$ ions may have bonded to –OH and –NH groups in the
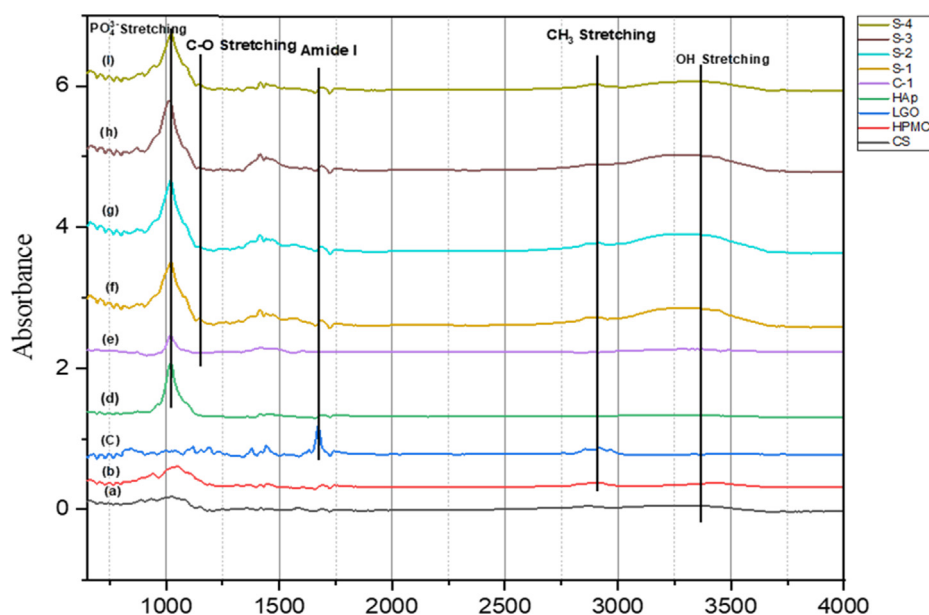


**Fig. 3** FTIR spectra of individual components and CS-HPMC-HAp-LGO composite scaffold (a) Pristine Chitosan, (b) Prisine HPMC, (c) Pristine LGO, (d) Pristine HAp, (e) Control scaffold with 0% LGO, (f) Sample-1 with 0.5% LGO, (g) Sample-2 with 1% LGO, (h) Sample-3 with 1.5% LGO, (i) Sample-4 with 2% LGO.

**Table 2** Characterization of FTIR spectra of CS-HPMC-HAp-LGO porous composite scaffolds.

| | Different Composition of Sample | | | | | Pristine Components | | | | Absorption Band | Intensity | Description |
|---|---|---|---|---|---|---|---|---|---|---|---|---|
| | C | S-1 | S-2 | S-3 | S-4 | Pure HAp | Pure CS | Pure HPMC | Pure LGO | | | |
| –OH Group | 3287 cm$^{-1}$ | 3272 cm$^{-1}$ | 3342 cm$^{-1}$ | 3274 cm$^{-1}$ | 3348 cm$^{-1}$ | – | 3285 cm$^{-1}$ | 3445 cm$^{-1}$ | 3524 cm$^{-1}$ | 3000–3600 cm$^{-1}$ | Broad & Strong | O-H (Free) Usually sharpO-H (H-bonded) Broad |
| $PO_4^{-3}$ Group | 1019 cm$^{-1}$ | 1021 cm$^{-1}$ | 1020 cm$^{-1}$ | 1018 cm$^{-1}$ | 1021 cm$^{-1}$ | 1020 cm$^{-1}$ | – | – | – | 1000–1100 cm$^{-1}$ | Strong | $\upsilon_3$ antisymmetric stretching vibration |
| $CO_3^{-2}$ Group | 870 cm$^{-1}$ | 873 cm$^{-1}$ | 873 cm$^{-1}$ | 870 cm$^{-1}$ | 870 cm$^{-1}$ | 874 cm$^{-1}$ | – | – | – | 870–880 cm$^{-1}$ | Weak | HAp Slightly Ca-deficient |
| C-H Bond of CH$_2$ | 1418 cm$^{-1}$ | 1414 cm$^{-1}$ | 1414 cm$^{-1}$ | 1416 cm$^{-1}$ | 1416 cm$^{-1}$ | – | 1417 cm$^{-1}$ | 1415 cm$^{-1}$ | – | 1360–1455 cm$^{-1}$ | Medium | C-H bond bending vibration of CH$_2$ |
| –C = O | 1643 cm$^{-1}$ | 1688 cm$^{-1}$ | 1685 cm$^{-1}$ | 1685 cm$^{-1}$ | 1689 cm$^{-1}$ | – | 1683 cm$^{-1}$ | – | – | 1630–1695 cm$^{-1}$ | Strong & Weak | Amide I stretching vibration band Due to C = O by incorporation of LG oil |
| C-O Bond | 1146 cm$^{-1}$ | 1145 cm$^{-1}$ | 1144 cm$^{-1}$ | 1142 cm$^{-1}$ | 1145 cm$^{-1}$ | – | 1148 cm$^{-1}$ | 1051 cm$^{-1}$ | 1118 cm$^{-1}$ | 1050–1150 cm$^{-1}$ | Weak | C-O bond stretching vibration |
| C–O–C cyclic | 880 cm$^{-1}$ | 886 cm$^{-1}$ | 885 cm$^{-1}$ | 888 cm$^{-1}$ | 893 cm$^{-1}$ | – | 936 cm$^{-1}$ | 942 cm$^{-1}$ | – | 900–950 cm$^{-1}$ | Medium & Weak | Six membered pyranose ring |
| $HO^-$ Group | – | – | – | – | – | 3570 cm$^{-1}$ | – | – | – | – | Weak & Broad | Absence refers to H-bonding |

organic phase. The C-H stretching bands of $CH_2$ and $CH_3$ appears in between 2850 $cm^{-1}$ to 3000 $cm^{-1}$ (Marques and L.A.d. Santos, L.F. Schopf, J.C.S.d. Fraga, , 2013; Bianchi et al., 2011) two strong peaks obtained at 2916 $cm^{-1}$ and 2966 $cm^{-1}$ in LGO spectrum which attribute C-H stretching vibration of $CH_2$, the absorption band obtained at 2871 $cm^{-1}$ and 2892 $cm^{-1}$ in CS and HPMC which attribute C-H stretching vibration of $CH_3$ respectively.

The presence of a broad –OH band in the 3000–3600 $cm^{-1}$ (Khan et al., 2015) range further confirms the existence of intramolecular H-bonds at the interface between inorganic and organic phases. The typical –OH/–NH bands is present in pristine CS at 3470 $cm^{-1}$, in HPMC at 3445 $cm^{-1}$, and in LGO at 3524 $cm^{-1}$ which is shifted to a shorter wavelength of $\sim$3250 $cm^{-1}$ in composite, confirming their involvement in interfacial H-bonding between organic and inorganic components of CS-HPMC-HAp-LGO composite.

The other major significant contribution from CS is the appearance of amide I band corresponding to (C = O) vibration of carbonyl group at $\sim$1683 $cm^{-1}$ and scissoring as well as bending vibrations of alkyl groups in between at 1360–1455 $cm^{-1}$ (Coates, 2000; Tang et al., 2003; Foroughi et al., 2012). The composite sample contains all of these wavebands. The stretching vibration bands of amide I due to C = O appear at 1671 $cm^{-1}$, 1683 $cm^{-1}$, 1692 $cm^{-1}$ in LG oil, CS and HPMC respectively. However, in all LGO incorporated samples the amide I stretching vibration band of C = O is shifted in between 1683 $cm^{-1}$ to 1689 $cm^{-1}$, which indicated the presence of LGO in composite scaffold. A small side band appear near the phosphate group at 1050 $cm^{-1}$ to 1150 $cm^{-1}$ which shows C-O bond stretching vibration in samples (Coates, 2000; Tang et al., 2003; Foroughi et al., 2012). The IR spectrum of CS, HPMC and LGO exhibits a small band of bending vibration of $CH_2$ in between at 1360 $cm^{-1}$ to 1455 $cm^{-1}$ (Khan et al., 2015) which shifted in between 1413 $cm^{-1}$ to 1444 $cm^{-1}$ due to LGO incorporation. The absorbance due to the C-O-C cyclic group of six membered pyranose ring is appears in between 900 and 950 $cm^{-1}$, in pure CS it appears at 936 $cm^{-1}$ and in HPMC at 942 $cm^{-1}$, in composites it shifts in between 880 and 895 $cm^{-1}$.

### 3.3. Mechanical properties

The mechanical strength of composite scaffold plays an important role in the development of bone tissue and protect the structure during the regeneration of tissues. In general pore sizes and porosity influence the strength of any composite scaffold. An ideal scaffold should have optimal porosity and strong enough to bear load during healing period in bone regeneration (Polo-Corrales et al., 2014). The compression strength of composite scaffold also depends on its composition (Zeeshan et al., 2018). Therefore, the mechanical strength is typically a major criterion for the selection of scaffold materials in BTE. Here, the compression strength of all HPMC crosslinked composite scaffold containing LGO 0% (C), 0.5% (S-1), 1% (S-2), 1.5% (S-3) and 2% (S-4) as shown in Fig. 4.

The presence of LGO in composite scaffold affects the compression strength, as it decreases the compression strength. As shown in Fig. 5, the composite scaffolds containing LGO indicate low specific compression strength and S-2 has minimum compression strength which is 0.06 MPa. The most important factor behind the low specific compression strength is the presence of LGO, due to which have decreased the cross-linking ability of HPMC. This behavior brought about low mechanical strength. However, the specific compression strength of C (0.27 MPa) and S-1 (0.23 MPa) composite scaffold was most satisfactory which comprise of 0% and 0.5% LGO respectively.

The composites of C and S-1 have low concentration of LGO which means that due to better cross-linking between HPMC with components, have high mechanical strength and low porosity. As the concentration of LGO was increased in other composite scaffolds, which is also increased their porosity. These behaviors lead to low mechanical properties. Whereas the remaining scaffolds with different LGO ratio have a strength in the range of 0.06–0.09 MPa. The better
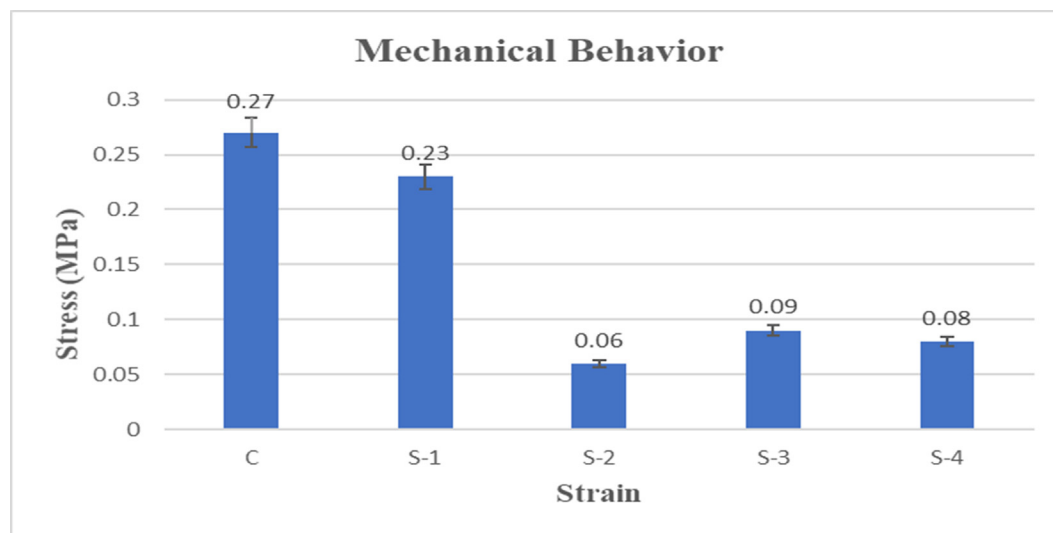


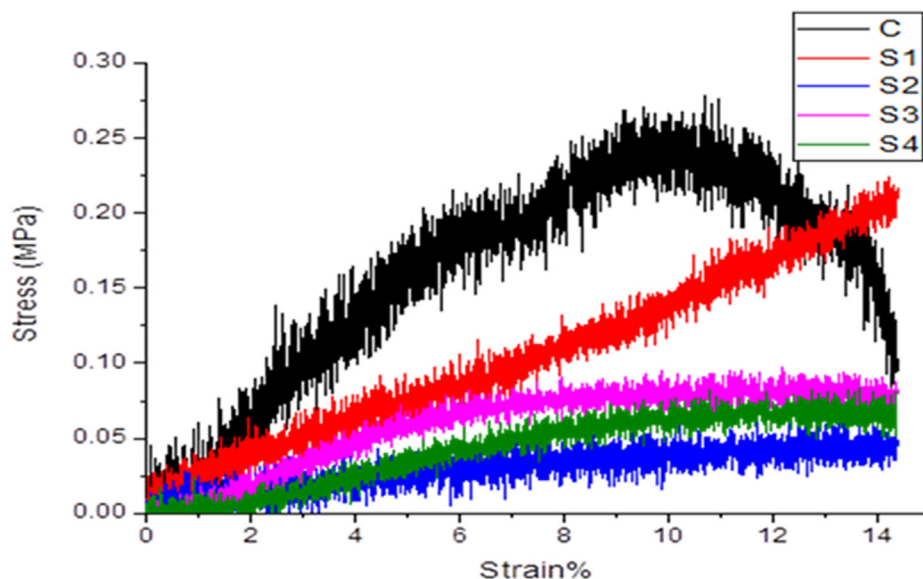**Fig. 4** Comparison of compression test of CS-HPMC-HAp-LGO composite scaffold.

**Fig. 5** Compression test of mechanical studies of CS-HPMC-HAp-LGO. —C, —S-1, —S-2, —S-3, —S-4.
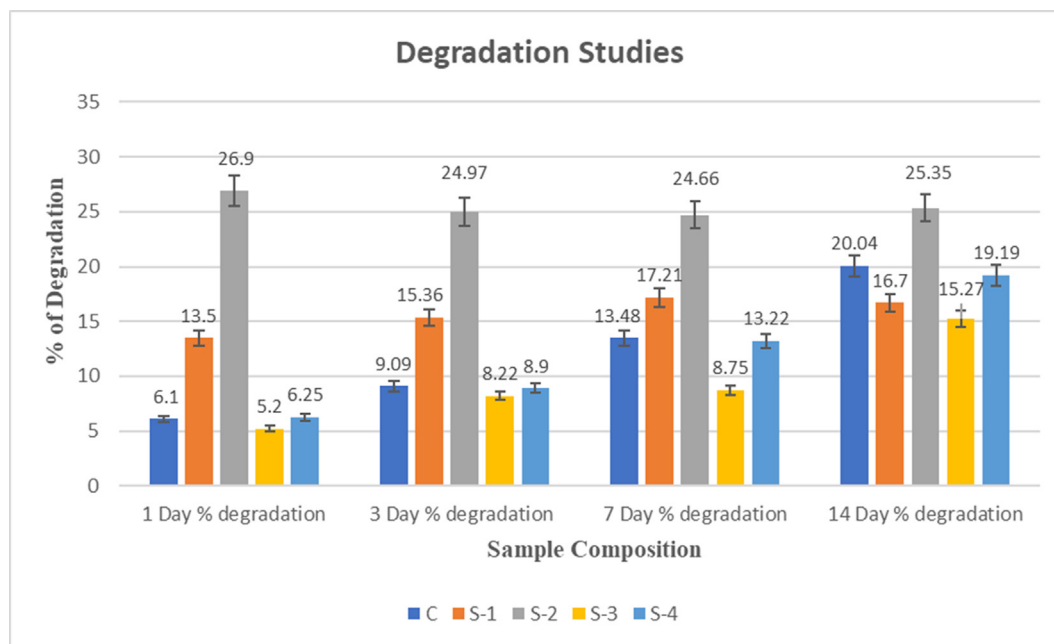


**Fig. 6** Degradation studies of CS-HPMC-HAp-LGO composites scaffold of for 1, 3, 7 & 14 days.

**Table 3** Degradation (%) of CS-HPMC-HAp-LGO composite scaffolds.

| S. code | Samples | Degradation (%) | | | | | | | |
|---------|---------|-------|-----------|-------|-----------|-------|-----------|--------|-----------|
| | | 1 Day | SD | 3 Day | SD | 7 Day | SD | 14 Day | SD |
| C | CS-HPMC-HAp-LGO (1/0.75/1.25/0) | 6.1 | ± 0.0770 | 9.09 | ± 0.5290 | 13.48 | ± 0.223 | 20.04 | ± 0.469 |
| S-1 | CS-HPMC-HAp-LGO (1/0.75/1.25/0.5) | 13.5 | ± 0.2932 | 15.36 | ± 0.2509 | 17.21 | ± 0.1248 | 16.70 | ± 0.2054 |
| S-2 | CS-HPMC-HAp-LGO (1/0.75/1.25/1) | 26.9 | ± 0.3858 | 24.97 | ± 0.2942 | 24.66 | ± 0.8730 | 25.35 | ± 0.2868 |
| S-3 | CS-HPMC-HAp-LGO (1/0.75/1.25/1.5) | 5.20 | ± 0.3300 | 8.22 | ± 0.1700 | 8.75 | ± 0.2749 | 15.27 | ± 0.0812 |
| S-4 | CS-HPMC-HAp-LGO (1/0.75/1.25/2) | 6.25 | ± 0.0943 | 8.9 | ± 0.1248 | 13.22 | ± 0.2056 | 19.19 | ± 0.1632 |

cross-linking between HPMC and HAp with chitosan exhibited highest compression strength in composite of C and S-1 (with low LGO concentrations).

### 3.4. Degradation behavior

As formation of new tissues occurs, the scaffolds ought to be degraded, which need to analyses for BTE application. The material used for the formation of scaffold ideally have following features; it should degrade in a controllable rate, and the product of degradation should be biocompatible and non-toxic (Vacanti and Langer, 1999; Wang, 2003). The biodegradation of scaffolds is a complex process in which the rate of degradation is affected by scaffold characteristics such as porosity, pore size, surface area, hydrophilicity, polymer structure, and so on. The mechanism of chitosan degradation in the body is enzymatic hydrolytic degradation via lysozymes (Ressler et al., 2022). The degradation profile of CS-HPMC-HAp with different concentration of LGO scaffolds is shown in Fig. 6, which was recorded for 2 weeks of incubation period in the presence of 100 µg/mL lysozyme solution (20,000 U/mL) in PBS medium at 37 °C. At day one, approximately 5% of degradation in all composite scaffolds were observed. The degradation rate was enhanced with time. However, the degradation of S-4 composite scaffold after 14 days was observed to be 19%, which revealed a slow degradation rate (Table 3). The degradation of S-4 composite scaffold gradually increased with the concentration of LGO in the sample. HPMC and LGO in PBS can be degraded that can alter the scaffold degradation activity. The bioactivity of composite scaffold improved as a result of degradation material because it helps to protect cells and a controlled degradation is one of important factors for BTE application.

The total % of degradation by all the composite scaffold of CS-HPMC-HAp-LGO after 14 days in PBS is approximately 19.19 ± 0.16%. However, in first week degradation rate is found to high, and then nearly consistent in the next weeks, which may be due to HPMC and CS. HPMC may degrade quickly than HAp and CS because of its hydrophilic nature (Khan et al., 2015; Jiang et al., 2008). However, although the quantity of HPMC compared to HAp and CS is low so after the first week the composite scaffold maintains a constant percentage degradation rate.

On the other hand, the hydrolytically unstable backbone of natural polymers like chitosan (Jiang et al., 2008; Venkatesan et al., 2012). that accelerates its % degradation rate in aqueous medium. The polymeric scaffold based on chitosan can be prepared which give appropriate surface for cell attachment, growth, withstand mechanical stresses and degrade. The PBS can hydrolyze the 1,4N-acetyl-glucosamine groups of CS chains. Due to its degradation amino sugars can be released into or excreted from the metabolic pathways of glycosaminoglycans and glycoprotein. The incorporation of ceramic particles increases the strength of material.

### 3.5. Swelling behavior

Swelling can promote cell penetration during in vitro tissue culture and enable cells to make their inner surfaces with the increase of the pore size (Teimouri et al., 2015; Mikos et al., 1993; Mulligan, 1993). The high degree of swelling causes a higher volume or surface ratio, which allows the better growth of cells. The inclusion of higher percentage of LGO in composite scaffold reduced the swelling ability (Table 4), which is because of the interaction of LGO with CS-HPMC-HAp. The results revealed that swelling ratio can be controlled in CS-HPMC-HAp composite scaffolds with the addition of LGO (Fig. 7).

Furthermore, the significant variation in swelling ratio could be attributed to hydrophobic character of LGO and Hap. So, HAp and LGO reduces the hydrophilicity of chitosan by linking with the hydrophilic $NH_2$ and OH. Water absorption into the interlinked pores of scaffolds is characterized by capillary action, as already shown (Gümüşderelioğlu et al., 2011). Generally swelling takes place as hydration takes place at the hydrophilic groups of material, and hydrophobic groups are leaving unaffected. Later on, as time passes, hydrophobic areas react with water, causing the scaffold to swell and more water is absorbed (Tahir et al., 2017). Scaffolds with the 0% LGO present higher swelling ratio as compared to the other scaffold that comprising of 0.5%, 1%, 1.5% and 2% LGO. Moreover, observation shows that swelling ratio was increased for each sample by the increase of immersion time. However, for the application of tissue engineering controlled swelling ratio is ideal.

### 3.6. Porosity

Biomaterial's porous structure plays an important role in the development of bones because it allows osteoblast as well as mesenchymal cells to migrate and spread along with vascularization. Phase separation, sintering depending, salt leaching, freeze drying and gas foaming are used to prepare the scaffolds and these are some common methods to established porosity in bio-material (Kumar et al., 2011; Karageorgiou and Kaplan, 2005; Hulbert et al., 1970; Moatary et al., 2017). Hence, poros-

**Table 4** Porosity, swelling ratio and density of CS-HPMC-HAp-LGO composite scaffolds.

| S. code | Composition | Porosity (%) | | Swelling ratio | | | | Density (gm/cm³) | |
|---------|-------------|--------------|---|----------------|---|------|---|------------------|---|
| | | | | 24 h | | 48 h | | | |
| C | CS-HPMC-HAp-LGO (1/0.75/1.25/0) | 66.5 | ± 0.0173 | 6.54 | ± 1.63 | 7.17 | ± 4.88 | 0.0382 | ± 0.2236 |
| S-1 | CS-HPMC-HAp-LGO (1/0.75/1.25/0.5) | 63.0 | ± 0.02 | 4.68 | ± 8.00 | 5.76 | ± 8.63 | 0.0458 | ± 0.100 |
| S-2 | CS-HPMC-HAp-LGO (1/0.75/1.25/1) | 64.3 | ± 0.01 | 4.69 | ± 5.95 | 6.14 | ± 4.58 | 0.0414 | ± 0.2828 |
| S-3 | CS-HPMC-HAp-LGO (1/0.75/1.25/1.5) | 68.75 | ± 0.00 | 5.81 | ± 3.06 | 6.36 | ± 2.49 | 0.0356 | ± 0.0000 |
| S-4 | CS-HPMC-HAp-LGO (1/0.75/1.25/2) | 74.25 | ± 0.0046 | 4.46 | ± 1.54 | 6.03 | ± 2.19 | 0.0286 | ± 0.1414 |
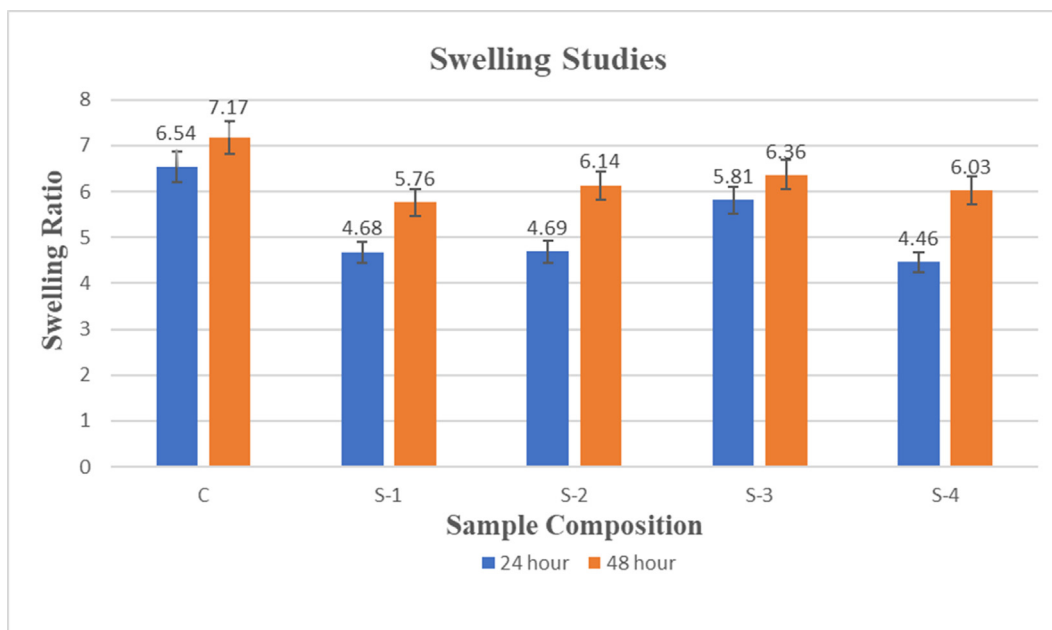
**Fig. 7** Swelling ratio of CS-HPMC-HAp-LGO composites scaffold after 24 & 48 h.

ity is a key factor in the utilization of scaffolds for applications of cell culture, because under ideal condition the cells can proliferate in the scaffold through pores and could be used for proliferation. The high porosity of scaffold helps them to transport oxygen and nutrient in their inner portion (Moatary et al., 2017). The porosity data of CS-HPMC-HAp-LGO composite scaffolds are shown in Table 4 and Fig. 8. From data, it was observed that by increasing the LGO contents in the scaffolds, the porosity was increased, which is due to LGO in the prepared samples (Table 4).

Density and porosity are essential parameters of scaffold in tissue engineering. Porous scaffold plays an important role in tissue repair by preserving the volume of tissue, promoting cell migration, providing temporary mechanical structure, and supplying proteins and genes (Venkatesan et al., 2012). High density may lead to higher mechanical stability and optimum

porosity is a permeability factor that promotes the distribution of cytokines and nutrients through the scaffold and elimination of waste material from scaffold (Tierney et al., 2009; Kavya et al., 2013). The use of LGO to produce composite material increases the porosity and decreases the density relative to CS-HPMC-HAp materials. The table 4 indicate densities of scaffolds, that due to LGO incorporation the density reduces to $0.0286 \text{ g/cm}^3$ and the inclusion of LGO along with HPMC raised porosity by 12% in comparison with CS-HPMC-HAp scaffold.

### 3.7. Antibacterial activity

Antibacterial activity of scaffold is necessary for successful implantation. Antibacterial activity of composite scaffold was evaluated by turbidimetric method. The bacterial viability
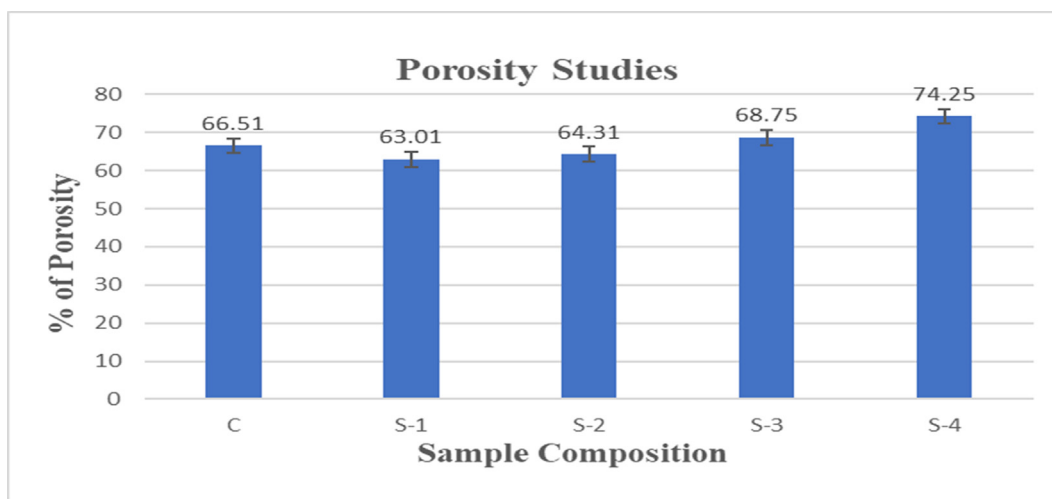


**Fig. 8** Percentage porosity of CS-HPMC-HAp-LGO composite scaffolds.

of cell percentage data is presented in Fig. 9. Overall, a decrease in the viability of *S. aureus* cells was seen for all composite scaffold of HPMC crosslinked containing LGO. The S-4 sample revealed a significant reduction in viable bacterial cell in the range of 5.52% to 18.71% in 2 to 24 h, respectively in comparison to negative control (Table 5). As the LGO concentration was increased, the activity was also enhanced that is due to incorporation of LGO content, resulting in reduction of viable bacterial cells. A significant reduction in % viable bacterial cell is observed for HPMC crosslinked composite materials containing a blend of LGO, HAp and CS, which can protect the tissues from bacterial attach during BTE application.

Studies revealed that the that LGO has antioxidant, antidepressant, sedative, astringent, antiseptic, nervous, fungicidal and bactericidal properties (McGuffin et al., 1997). This study was therefore conducted to determine the antibacterial behavior of LGO against pathogenic bacteria. As increase in LGO concentration resulted in improved porosity as well as possibly decreased mechanical strength, which may be useful in releasing the LGO content, resulting in reduction of viable bacterial cells. LGO consists of many chemical components, the main components i.e. are myrcene, geraniol, geranyl acetate, neral, citronellal, nerol and traces of citral and limonene and its

antibacterial action on the bacterial cell may have many targets of action. Citral component of LGO is more effective against *S. Aureus* and can improve the cell permeability. However, geraniol effect the cytoplasmic membranes.

The LGO and its vital components may influence the cytoplasmic structure of tested bacterial cell more than cell wall. Previous studies reported that, in the primary stage, the LGO may possibly bind on bacterial cell membrane and then invade into cell wall which cause swelling as well as cytoplasmic membranes damage, as a result the cells become shrink in response against the LGO. In the second stage, citral components reveal the empty spaces. These may be due to LGO penetration, or cellular changes resulting from oil exposure. Geraniol demonstrates minor damage to the cytoplasmic membrane and it may coagulate the cell wall and cytoplasm (Aiemsaard et al., 2011). Hence, destroys structure of bacterial cell. However, in addition to citral and geraniol, many minor chemicals of LGO can also modulate their antibacterial effect, like geranyl acetate and linalool, that have been stated to be weak activity (Dorman and Deans, 2000; Prashar et al., 2003). So that, we can say the obtained HPMC crosslinked composite materials containing a blend of LGO, HAp and CS that may be acceptable for the preparation of materials which can kill pathogenic bacteria *S. Aureus*.
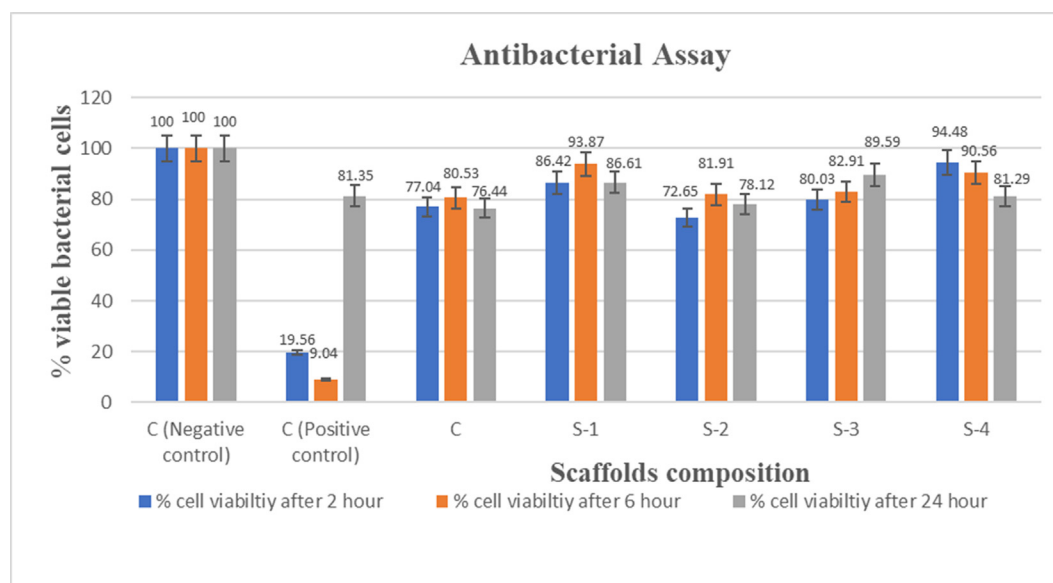


**Fig. 9** Antibacterial activity of Control (C), Sample-1 (S-1), Sample-2 (S-2), Sample-3 (S-3), Sample-4 (S-4) scaffolds against *S. aureus* at 2 h, 6 h and 24 h.

**Table 5** Antibacterial activity of CS-HPMC-HAp-LGO composite scaffolds.

| Code | Samples | Viable (%) bacterial cell 2 h | | Viable (%) bacterial cell 6 h | | Viable (%) bacterial cell 24 h | |
|---|---|---|---|---|---|---|---|
| C⁻ | C⁻ (-ve Control without sample) | 100 | ±0.000 | 100 | ±0.000 | 100 | ±0.000 |
| C⁺⁺ | C⁺⁺ (+ve control with commercial disk) | 19.56 | ±0.009 | 9.04 | ±0.006 | 81.35 | ±0.017 |
| C | CS-HPMC-HAp-LGO (1/0.75/1.25/0) | 77.04 | ±0.417 | 80.53 | ±0.002 | 76.44 | ±0.011 |
| S-1 | CS-HPMC-HAp-LGO (1/0.75/1.25/0.5) | 86.42 | ±0.024 | 93.87 | ±0.001 | 86.61 | ±0.025 |
| S-2 | CS-HPMC-HAp-LGO (1/0.75/1.25/1) | 72.65 | ±0.002 | 81.91 | ±0.039 | 78.12 | ±0.052 |
| S-3 | CS-HPMC-HAp-LGO (1/0.75/1.25/1.5) | 80.03 | ±0.001 | 82.90 | ±0.025 | 89.59 | ±0.050 |
| S-4 | CS-HPMC-HAp-LGO (1/0.75/1.25/2) | 94.48 | ±0.023 | 90.56 | ±0.034 | 81.29 | ±0.008 |

**Table 6** Cell viability (%) of composite scaffolds of CS-HPMC-HAp-LGO.

| S. code | Composition | % cell viability At Day 1 | | % cell viability At Day 3 | | % cell viability At Day 7 | |
|---------|-------------|-----|------|-----|------|-----|------|
| TCP | TCP | 100 | ± 0.00 | 100 | ± 0.000 | 100 | ± 0.000 |
| C | CS-HPMC-HAp-LGO (1/0.75/1.25/0) | 101.4 | ± 0.041 | 93.71 | ± 0.000 | 117.9 | ± 0.039 |
| S-1 | CS-HPMC-HAp-LGO (1/0.75/1.25/0.5) | 101.1 | ± 0.003 | 95.79 | ± 0.007 | 93.46 | ± 0.004 |
| S-2 | CS-HPMC-HAp-LGO (1/0.75/1.25/1) | 96.88 | ± 0.004 | 96.11 | ± 0.003 | 116.3 | ± 0.026 |
| S-3 | CS-HPMC-HAp-LGO (1/0.75/1.25/1.5) | 93.89 | ± 0.004 | 95.59 | ± 0.004 | 99.3 | ± 0.004 |
| S-4 | CS-HPMC-HAp-LGO (1/0.75/1.25/2) | 95.97 | ± 0.013 | 95.98 | ± 0.003 | 101.3 | ± 0.012 |
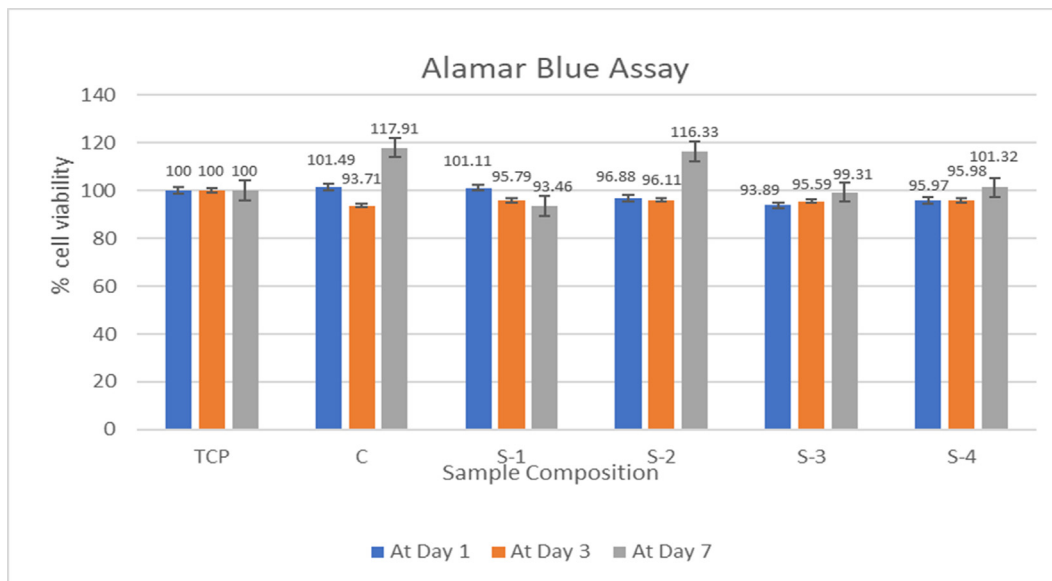


**Fig. 10** Cytotoxicity study of CS-HPMC-HAp-LGO composites scaffold for 1, 3 & 7 days.

### 3.8. Cytotoxicity analysis

The proliferation and mitochondrial activity of pre-osteoblast (MC3T3E1) cell was examined using Alamar Blue method. The % of cell viability on CS-HPMC-HAp-LGO composite scaffold was evaluated for 1, 3 and 7 days (Table 6). Optical density was checked and responses thus observed are shown in Fig. 10. The results showed that the CS-HPMC-HAp-LGO composite scaffolds were non-toxic, which could be biocompatible and can promote cell proliferation. Results showed that cells on all five scaffolds were viable after 7 days of growth and their concentration also did not change in 7 days.

BTE Scaffolds need highly porous network that ensure the cellular environment led to proliferation, growth of tissue, cell attachment and sufficient nutrient flow (Dhandayuthapani et al., 2011; Lee et al., 2014). Alamar Blue assay was used to demonstrate the cell proliferation and cell viability effects of the respective scaffolds. In this research, MC3T3-E1 pre-osteoblast cells were cultured on five various scaffolds. The only difference between these five HPMC crosslinked scaffold is the concentration of LGO. The % of cell viability on CS-HPMC-HAp-LGO composite scaffold was evaluated for 1, 3 and 7 days. It is recognized that composite scaffold of CS-HPMC-HAp is highly biocompatible at day 7, and the proportion of viable cells in CS-HPMC-HAp is greater than others at this day, as shown in Fig. 10. However, in other samples that contain various concentration of LGO, the number of viable cells is not enough lower which indicate toxicity. It is found that, after 7 days of incubation, all of the HPMC crosslinked composite scaffolds with 93–117% of cell viability remains nontoxic towards MC3T3-E1 pre-osteoblast cells line.

A significant increase in sample C and S-2 cell proliferation from day 3 to 7 may have been due to the fact that by day 3 the cells have become accustomed to surrounding environment which strongly supports the proliferation of cells. The lower proliferation of cells in S1 may be due to topography of scaffold network limiting the proliferative ability of the MC3T3-E1 pre-osteoblast cells at day 3 and 7, as shown in Fig. 10. Another possibility can be the aggregates produced by pre-osteoblast cells, whereas secretions of the extracellular matrix led to reduce the supplies of nutrient, thus decreasing the cellular metabolic activity (Zeeshan et al., 2018). Generally, we can say that all these composite scaffolds to be biocompatible with their various cell attachment capability.

### 4. Conclusion

Biomedical research has explored the possibilities of creating scaffolds that could closely resemble to the physiological environment. A novel composite scaffolds based on HPMC crosslinked chitosan-hydroxyapatite containing Lemongrass oil for possible BTE applications has been presented using freeze gelation technique. In this research, a series of chemical and physical properties of composite scaffolds based on CS-HPMC-HAp-LGO were tested, and cell viability and antibacterial activity was evaluated for the scaffolds. The pre-

pared scaffolds were characterized with Fourier Transform Infrared Spectroscopy and fatigue test. The presence of molecular interaction and individual components is confirmed by Fourier Transform Infrared Spectroscopy. The research findings revealed that all composite scaffolds of CS-HPMC-HAp-LGO with porous network have significant antibacterial activity and good viability with cell. Studies of cell viability showed no indication of toxicity. As increase in LGO concentration resulted in improved porosity as well as possibly decreased mechanical strength and decreased density. The in-vitro cells culture showed that MC3T3-E1 cells grown on the composite scaffolds of CS-HPMC-HAp-LGO had positive potential for proliferation. In the end, we have successfully developed a bio-mimic composite scaffold that has identical physicochemical characteristic as natural bone also including commendable osteogenic properties that make it a promising material in the field of Bone tissue engineering.

## References

Sanjay, V., Menon, H., Dhivya, S., Selvamurugan, N., 2017. Effects of flavonoids incorporated biological macromolecules based scaffolds in bone tissue engineering. Int. J. Biol. Macromol. 110, 74–87.

Chen, F.-M., Jin, Y., 2010. Periodontal tissue engineering and regeneration: current approaches and expanding opportunities. Tissue Engineering Part B: Reviews 16 (2), 219–255.

Eftekhari, A., Ahmadian, E., Azami, A., Johari-Ahar, M., Eghbal, M. A., 2018. Protective effects of coenzyme Q10 nanoparticles on dichlorvos-induced hepatotoxicity and mitochondrial/lysosomal injury. Environ. Toxicol. 33 (2), 167–177.

Asghar, M.S., Li, J., Ahmed, I., Ghazanfar, U., Irshad, M.S., Idrees, M., Haq, Z., Rizwan, M., Sheikh, F., Yasmeen, F., 2021. Antioxidant, and enhanced flexible nano porous scaffolds for bone tissue engineering applications. Nano Select 2 (7), 1356–1367.

Wu, D., Wang, X., Sun, H., 2018. The role of mitochondria in cellular toxicity as a potential drug target. Springer, 87–91.

Abbasi, M.S., Irshad, M.S., Arshad, N., Ahmed, I., Idrees, M., Ahmad, S., Wei, Z., Sharaf, M., M.d., 2020. Al Firdausi, Biomaterial-induced stable resistive switching mechanism in TiO2 thin films: the role of active interstitial sites/ions in minimum current leakage and superior bioactivity. ACS Omega 5 (30), 19050–19060.

Balagangadharan, K., Dhivya, S., Selvamurugan, N., 2017. Chitosan based nanofibers in bone tissue engineering. Int. J. Biol. Macromol. 104, 1372–1382.

Saravanan, S., Leena, R., Selvamurugan, N., 2016. Chitosan based biocomposite scaffolds for bone tissue engineering. Int. J. Biol. Macromol. 93, 1354–1365.

Shuai, C., Guo, W., Wu, P., Yang, W., Hu, S., Xia, Y., Feng, P., 2018. A graphene oxide-Ag co-dispersing nanosystem: Dual synergistic effects on antibacterial activities and mechanical properties of polymer scaffolds. Chem. Eng. J. 347, 322–333.

Feng, P., Kong, Y., Yu, L., Li, Y., Gao, C., Peng, S., Pan, H., Zhao, Z., Shuai, C., 2019. Molybdenum disulfide nanosheets embedded with nanodiamond particles: co-dispersion nanostructures as reinforcements for polymer scaffolds. Applied Mater. Today 17, 216–226.

Heise, U., Osborn, J., Duwe, F., 1990. Hydroxyapatite ceramic as a bone substitute. Int. Orthop. 14 (3), 329–338.

Shuai, C., Peng, B., Feng, P., Yu, L., Lai, R., Min, A., 2021. In situ synthesis of hydroxyapatite nanorods on graphene oxide nanosheets and their reinforcement in biopolymer scaffold. J. Adv. Res.

Shuai, C., Yang, W., Feng, P., Peng, S., Pan, H., 2021. Accelerated degradation of HAP/PLLA bone scaffold by PGA blending facilitates bioactivity and osteoconductivity. Bioact. Mater. 6 (2), 490–502.

Panda, S., Biswas, C.K., Paul, S., 2021. A comprehensive review on the preparation and application of calcium hydroxyapatite: A special focus on atomic doping methods for bone tissue engineering. Ceram. Int. 47 (20), 28122–28144.

Ressler, A., Žužić, A., Ivanišević, I., Kamboj, N., Ivanković, H., 2021. Ionic substituted hydroxyapatite for bone regeneration applications. A Review, Open Ceramics 100122.

Feng, P., Wu, P., Gao, C., Yang, Y., Guo, W., Yang, W., Shuai, C., 2018. A multimaterial scaffold with tunable properties: toward bone tissue repair. Adv. Sci. 5 (6), 1700817.

Hong, S.-C., Yoo, S.-Y., Kim, H., Lee, J., 2017. Chitosan-based multifunctional platforms for local delivery of therapeutics. Mar. Drugs 15 (3), 60.

P. Giotra, S.K. Singh, Chitosan: An emanating polymeric carrier for drug delivery, Handbook of Polymers for Pharmaceutical Technologies: Biodegradable Polymers; Thakur, VK, Thakur, MK, Eds (2015) 33-39.

Siepmann, J., Peppas, N.A., 2012. Modeling of drug release from delivery systems based on hydroxypropyl methylcellulose (HPMC). Adv. Drug Deliv. Rev. 64, 163–174.

Pawlak, A., Mucha, M., 2003. Thermogravimetric and FTIR studies of chitosan blends. Thermochim Acta 396 (1–2), 153–166.

Mahmoudian, M., Ganji, F., 2017. Vancomycin-loaded HPMC microparticles embedded within injectable thermosensitive chitosan hydrogels. Prog. Biomater. 6 (1), 49–56.

Ahmadian, E., Eftekhari, A., Dizaj, S.M., Sharifi, S., Mokhtarpour, M., Nasibova, A.N., Khalilov, R., Samiei, M., 2019. The effect of hyaluronic acid hydrogels on dental pulp stem cells behavior. Int. J. Biol. Macromol. 140, 245–254.

Hafsa, J., M. ali Smach, M.R.B. Khedher, B. Charfeddine, K. Limem, H. Majdoub, S. Rouatbi,, 2016. Physical, antioxidant and antimicrobial properties of chitosan films containing Eucalyptus globulus essential oil, LWT-Food. Science and Technology 68, 356–364.

Stegăruş, D.I., Lengyel, E., 2017. The antimicrobial effect of essential oils upon certain nosocomial bacteria. International Multidisciplinary Scientific GeoConference: SGEM 17, 1089–1095.

Jian-Ping, B., Li, P., Xi-Xi, X., Ting, W., Fei, L., 2018. Anti-rheumatoid arthritic effect of volatile components in notopterygium incisum in rats via anti-inflammatory and anti-angiogenic activities. Chinese J. Natural Medicines 16 (12), 926–935.

Zhang, Z., Zheng, Y., Zhang, L., Mani, M.P., Jaganathan, S.K., 2019. In vitro blood compatibility and bone mineralization aspects of polymeric scaffold laden with essential oil and metallic particles for bone tissue engineering. Int. J. Polym. Anal. Charact. 24 (6), 504–516.

Florea, A.D., Dănilă, E., Constantinescu, R.R., Kaya, M.A., Kaya, A. D., Coară, G., Albu, L., Chelaru, C., 2018. COMPOSITE SCAFFOLDS FOR BONE REGENERATION MADE OF COLLAGEN/HYDROXY APATITE/EUCALYPTUS ESSEN-TIAL OIL. In: International Conference on Advanced Materials and Systems (ICAMS), The National Research & Development Institute for Textiles and Leather-INCDTP, pp. 93–98.

Khan, A.F., Afzal, A., Chaudhary, A.A., Saleem, M., Shahzadi, L., Jamal, A., Yar, M., Habib, A., 2015. (Hydroxypropyl) methylcel-lulose mediated synthesis of highly porous composite scaffolds for trabecular bone repair applications. Sci. Adv. Mater. 7 (6), 1177–1186.

Ressler, A., Gudelj, A., Zadro, K., Antunović, M., Cvetnić, M., Ivanković, M., Ivanković, H., 2020. From bio-waste to bone substitute: synthesis of biomimetic hydroxyapatite and its use in chitosan-based composite scaffold preparation. Chem. Biochem. Eng. Q. 34 (2), 59–71.

Currey, J., Butler, G., 1975. The mechanical properties of bone tissue in children, The Journal of bone and joint surgery. American 57 (6), 810–814.

Hing, K., Best, S., Bonfield, W., 1999. Characterization of porous hydroxyapatite. J. Mater. Sci. - Mater. Med. 10 (3), 135–145.

Hodgskinson, R., Currey, J., 1990. The effect of variation in structure on the Young's modulus of cancellous bone: a comparison of human and non-human material. Proc. Inst. Mech. Eng. [H] 204 (2), 115–121.

Shalumon, K., Anulekha, K., Chennazhi, K.P., Tamura, H., Nair, S., Jayakumar, R., 2011. Fabrication of chitosan/poly (caprolactone) nanofibrous scaffold for bone and skin tissue engineering. Int. J. Biol. Macromol. 48 (4), 571–576.

Amalraj, A., Haponiuk, J.T., Thomas, S., Gopi, S., 2020. Preparation, characterization and antimicrobial activity of polyvinyl alcohol/gum arabic/chitosan composite films incorporated with black pepper essential oil and ginger essential oil. Int. J. Biol. Macromol. 151, 366–375.

Altiok, D., Altiok, E., Tihminlioglu, F., 2010. Physical, antibacterial and antioxidant properties of chitosan films incorporated with thyme oil for potential wound healing applications. J. Mater. Sci. - Mater. Med. 21 (7), 2227–2236.

Güneş, S., Tıhmınlıoğlu, F., 2017. Hypericum perforatum incorpo-rated chitosan films as potential bioactive wound dressing material. Int. J. Biol. Macromol. 102, 933–943.

Song, X., Zuo, G., Chen, F., 2018. Effect of essential oil and surfactant on the physical and antimicrobial properties of corn and wheat starch films. Int. J. Biol. Macromol. 107, 1302–1309.

C.D. Grande Tovar, J.I. Castro, C.H. Valencia Llano, D.P. Navia Porras, J. Delgado Ospina, M.E. Valencia Zapata, J. Herminsul Mina Hernandez, M.N. Chaur, Synthesis, characterization, and histological evaluation of chitosan-Ruta graveolens essential oil films, Molecules 25(7) (2020) 1688.

Murphy, C.M., O'Brien, F.J., 2010. Understanding the effect of mean pore size on cell activity in collagen-glycosaminoglycan scaffolds. Cell adhesion & migration 4 (3), 377–381.

Rehman, I., Bonfield, W., 1997. Characterization of hydroxyapatite and carbonated apatite by photo acoustic FTIR spectroscopy. J. Mater. Sci. - Mater. Med. 8 (1), 1–4.

Swain, S., Bhattacharyya, S., Sarkar, D., 2011. Preparation of porous scaffold from hydroxyapatite powders. Mater. Sci. Eng., C 31 (6), 1240–1244.

Mobasherpour, I., Heshajin, M.S., Kazemzadeh, A., Zakeri, M., 2007. Synthesis of nanocrystalline hydroxyapatite by using precipitation method. J. Alloy. Compd. 430 (1–2), 330–333.

Antonakos, A., Liarokapis, E., Leventouri, T., 2007. Micro-Raman and FTIR studies of synthetic and natural apatites. Biomaterials 28 (19), 3043–3054.

Delgado-López, J.M., Iafisco, M., Rodríguez, I., Tampieri, A., Prat, M., Gómez-Morales, J., 2012. Crystallization of bioinspired citrate-functionalized nanoapatite with tailored carbonate content. Acta Biomater. 8 (9), 3491–3499.

Meejoo, S., Maneeprakorn, W., Winotai, P., 2006. Phase and thermal stability of nanocrystalline hydroxyapatite prepared via microwave heating. Thermochim Acta 447 (1), 115–120.

Marques, D.R., L.A.d. Santos, L.F. Schopf, J.C.S.d. Fraga,, 2013. Analysis of poly (lactic-co-glycolic acid)/poly (isoprene) polymeric blend for application as biomaterial. Polímeros 23 (5), 579–584.

Bianchi, S.E., Angeli, V.W., et al, 2011. Evaluation of the solubility of the HPMC: PVA blends in biological fluids in vitro. Mater. Res. 14, 166–171.

Coates, J., 2000. Interpretation of infrared spectra, a practical approach. Citeseer.

Tang, E., Huang, M., Lim, L.Y., 2003. Ultrasonication of chitosan and chitosan nanoparticles. Int. J. Pharm. 265 (1–2), 103–114.

Foroughi, M.R., Karbasi, S., Ebrahimi-Kahrizsangi, R., 2012. Phys-ical and mechanical properties of a poly-3-hydroxybutyrate-coated nanocrystalline hydroxyapatite scaffold for bone tissue engineering. J. Porous Mater. 19 (5), 667–675.

Polo-Corrales, L., Latorre-Esteves, M., Ramirez-Vick, J.E., 2014. Scaffold design for bone regeneration. J. Nanosci. Nanotechnol. 14 (1), 15–56.

Zeeshan, R., Mutahir, Z., Iqbal, H., Ali, M., Iqbal, F., Ijaz, K., Sharif, F., Shah, A.T., Chaudhry, A.A., Yar, M., 2018. Hydroxypropy-lmethyl cellulose (HPMC) crosslinked chitosan (CH) based scaf-folds containing bioactive glass (BG) and zinc oxide (ZnO) for alveolar bone repair. Carbohydr. Polym. 193, 9–18.

Vacanti, J.P., Langer, R., 1999. Tissue engineering: the design and fabrication of living replacement devices for surgical reconstruction and transplantation. The lancet 354, S32–S34.

Wang, M., 2003. Developing bioactive composite materials for tissue replacement. Biomaterials 24 (13), 2133–2151.

Ressler, A., Antunović, M., Teruel-Biosca, L., Ferrer, G.G., Babić, S., Urlić, I., Ivanković, M., Ivanković, H., 2022. Osteogenic differen-tiation of human mesenchymal stem cells on substituted calcium phosphate/chitosan composite scaffold. Carbohydr. Polym. 277, 118883.

Jiang, L., Li, Y., Wang, X., Zhang, L., Wen, J., Gong, M., 2008. Preparation and properties of nano-hydroxyapatite/chitosan/car-boxymethyl cellulose composite scaffold. Carbohydr. Polym. 74 (3), 680–684.

Venkatesan, J., Pallela, R., Bhatnagar, I., Kim, S.-K., 2012. Chitosan–amylopectin/hydroxyapatite and chitosan–chondroitin sulphate/hydroxyapatite composite scaffolds for bone tissue engineering. Int. J. Biol. Macromol. 51 (5), 1033–1042.

Teimouri, A., Azadi, M., Emadi, R., Lari, J., Chermahini, A.N., 2015. Preparation, characterization, degradation and biocompatibility of different silk fibroin based composite scaffolds prepared by freeze-drying method for tissue engineering application. Polym. Degrad. Stab. 121, 18–29.

Mikos, A.G., Sarakinos, G., Lyman, M.D., Ingber, D.E., Vacanti, J. P., Langer, R., 1993. Prevascularization of porous biodegradable polymers. Biotechnol. Bioeng. 42 (6), 716–723.

Mulligan, R.C., 1993. The basic science of gene therapy. Science 260 (5110), 926–932.

Gümüşderelioğlu, M., Erce, D., Demirtaş, T.T., 2011. Superporous polyacrylate/chitosan IPN hydrogels for protein delivery. J. Mater. Sci. - Mater. Med. 22 (11), 2467–2475.

Tahir, N., Bhatti, H.N., Iqbal, M., Noreen, S., 2017. Biopolymers composites with peanut hull waste biomass and application for Crystal Violet adsorption. Int. J. Biol. Macromol. 94, 210–220.

Kumar, P.S., Srinivasan, S., Lakshmanan, V.-K., Tamura, H., Nair, S., Jayakumar, R., 2011. Synthesis, characterization and cytocom-patibility studies of α-chitin hydrogel/nano hydroxyapatite com-posite scaffolds. Int. J. Biol. Macromol. 49 (1), 20–31.

Karageorgiou, V., Kaplan, D., 2005. Porosity of 3D biomaterial scaffolds and osteogenesis. Biomaterials 26 (27), 5474–5491.

Hulbert, S., Young, F., Mathews, R., Klawitter, J., Talbert, C., Stelling, F., 1970. Potential of ceramic materials as permanently implantable skeletal prostheses. J. Biomed. Mater. Res. 4 (3), 433–456.

Moatary, A., Teimouri, A., Bagherzadeh, M., Chermahini, A.N., Razavizadeh, R., 2017. Design and fabrication of novel chitin hydrogel/chitosan/nano diopside composite scaffolds for tissue engineering. Ceram. Int. 43 (2), 1657–1668.

Tierney, C.M., Haugh, M.G., Liedl, J., Mulcahy, F., Hayes, B., O'Brien, F.J., 2009. The effects of collagen concentration and crosslink density on the biological, structural and mechanical properties of collagen-GAG scaffolds for bone tissue engineering. J. Mech. Behav. Biomed. Mater. 2 (2), 202–209.

Kavya, K., Jayakumar, R., Nair, S., Chennazhi, K.P., 2013. Fabrication and characterization of chitosan/gelatin/nSiO2 composite scaffold for bone tissue engineering. Int. J. Biol. Macromol. 59, 255–263.

McGuffin, M., Hobbs, C., Upton, R., Goldberg, A., 1997. Botanical Safety Handbook. CRC Press, LLC, American Herbal Products Association, Boca Raton, Floride.

Aiemsaard, J., Aiumlamai, S., Aromdee, C., Taweechaisupapong, S., Khunkitti, W., 2011. The effect of lemongrass oil and its major components on clinical isolate mastitis pathogens and their mechanisms of action on Staphylococcus aureus DMST 4745. Res. Vet. Sci. 91 (3), e31–e37.

Dorman, H.D., Deans, S.G., 2000. Antimicrobial agents from plants: antibacterial activity of plant volatile oils. J. Appl. Microbiol. 88 (2), 308–316.

Prashar, A., Hili, P., Veness, R.G., Evans, C.S., 2003. Antimicrobial action of palmarosa oil (Cymbopogon martinii) on Saccharomyces cerevisiae. Phytochemistry 63 (5), 569–575.

Dhandayuthapani, B., Yoshida, Y., Maekawa, T., Kumar, D.S., 2011. Polymeric scaffolds in tissue engineering application: a review. International J. Polymer Sci. 2011.

Lee, J.S., Baek, S.D., Venkatesan, J., Bhatnagar, I., Chang, H.K., Kim, H.T., Kim, S.-K., 2014. In vivo study of chitosan-natural nano hydroxyapatite scaffolds for bone tissue regeneration. Int. J. Biol. Macromol. 67, 360–366.